Eur. Phys. J. B **3**, 45–57 (1998)

THE EUROPEAN PHYSICAL JOURNAL B

Behavior of one inelastic ball bouncing repeatedly off the ground

E. Falcon[a], C. Laroche, S. Fauve, and C. Coste

Laboratoire de Physique, École Normale Supérieure de Lyon, 46 allée d'Italie, 69364 Lyon Cedex 07, France

Received: 2 December 1997 / Accepted: 5 March 1998

Abstract. An experimental study of the behavior of one bead bouncing repeatedly off a static flat horizontal surface is presented. We observe that the number of bounces made by the bead is finite. When the duration between two successive bounces becomes of the order of the impact duration, the bead no longer bounces but oscillates on the elastically deformed surface before coming to rest. This transition is explained with a modified Hertz interaction law in which gravity is taken into account during the interaction. For each bounce, measurement of both the duration of collision and the restitution coefficient have been done. The effective restitution coefficient is essentially constant and close to 1 during almost all bounces before decreasing to zero when the impact velocity vanishes. This is due to an interplay between gravity and viscoelastic dissipation.

PACS. 46.10.+z Mechanics of discrete systems – 83.70.Fn Granular solids

1 Introduction

Recently, considerable attention has been devoted to the study of granular materials (for an overview see Refs. [1,2]). In particular, granular flows give rise to a variety of phenomena, such as convection [3,4], surface excitations [5–7] and fluidization [8–10]. In all cases, the inelastic character of collisions between two grains or between a grain and a wall of the container strongly affects the dynamical behavior of such dissipative media. Very large scale examples of granular gases are the planetary rings, *e.g.*, those of Saturn, whose dynamics are basically determined by the properties of the inelastic collisions occurring between particles composing the rings [11–13].

While over the years many attempts [10,14–17] have been made to formalize the complex rheology of dissipative granular gases, several recent theoretical and numerical studies of the role of inelastic collisions in such media have shown surprising dynamics. For example, when an inelastic hard core granular gas is initially in a thermalized state and then freely evolves without the addition of energy, the inelastic dynamic of such a "cooling" granular system results in the evolution through four different regimes (kinetic, shearing, clustered and collapsed) [18], two of which leads to structures in 1–D or 2–D: Clusters [19,20] or "inelastic collapse" [20–23]. The inelastic collapse is a special type of clustering in which a group of particles undergo an infinite number of collisions occurring in a finite time. The result of inelastic collapse is that the particles actually come into contact, whereas in a cluster the particles are close together, but not in contact. Most people working on inelastic collapse consider that this phenomenon is qualitatively akin to the behavior of one inelastic ball bouncing repeatedly off the ground. Indeed, if during each bounce, the collision is assumed instantaneous and inelastic with constant restitution coefficient, it is easy to show that the ball comes to rest after an infinite number of bounces in a finite time. This theoretical feature will be called hereafter the "collisional singularity".

As well as the role of inelastic collisions, the role of contacts between grains is basic for the study of granular materials since energy dissipation takes place mostly at those contacts. In this respect, normal binary collisions may facilitate the understanding of such contact's properties, and are a first step toward multibodies collision [24]. Although there have been many works [25–27] dealing with the dynamic of inelastic binary collisions and a lot of measurements of the energy loss in such collisions [11–14,27–38], there is a considerable scatter in existing data. At high impact velocities, *i.e.*, when fully plastic deformations occur, the evolution of the restitution coefficient, ϵ, as a function of the impact velocity is well known both experimentally [27,35] and theoretically [26,35]. However, at very low incident velocities, both the behavior of ϵ with the impact velocity and the mechanisms responsible for a possible dissipation are still open problems.

In this paper, we analyse experimentally the behavior of one bead bouncing repeatedly off a stationary massive flat surface. The bead is dropped, without initial velocity, from a fixed height above this surface. This system is well adapted to study how the collisional singularity and, in a wider sense, the inelastic collapse, are "smoothed" when the simplifying theoretical assumptions are replaced

[a] e-mail: efalcon@physique.ens-lyon.fr

by realistic experimental conditions. Obviously, an infinite number of bounces occurring in a finite time is not expected in an experiment since the duration of a collision is non zero. However, it is not trivial to understand how the collisional singularity is removed, *i.e.*, which is the saturation mechanism. Finally, this problem raises several questions: Does the duration between two successive bounces tend to zero? How many times does the bead bounce before coming to rest? How do the restitution coefficient and the duration of impact, scale when the impact velocity of the bead tends to zero? What are the mechanisms of energy loss during a bounce at very low impact velocity?

This paper is organized as follows. The elementary model of an inelastic bead bouncing on a flat surface is recalled in Section 2. In this model each collision is assumed instantaneous, and the bead comes to rest, after an infinite number of bounces, in a finite time. However, experimental results will show that the finite duration of bounces cannot be neglected, so that the elementary model does not apply. The experimental setup is presented in Section 3. The experimental results are reported and discussed in Section 4. We observe that when the duration of a collision is of the order of the flight time between two successive bounces, the bead no longer bounces but oscillates on the plane with a characteristic period. Because of dissipation, the oscillation amplitude decreases to zero until the bead comes to rest. For each bounce, measurement of both the duration of collision and the restitution coefficient have been done. The restitution coefficient is found to be essentially constant and close to 1 during almost all bounces till it decreases when the impact velocity tends to zero, *i.e.*, for the last bounces. The duration of collision is in fair agreement with the prediction of Hertz's theory [39] during almost all bounces, but becomes longer at very small impact velocities, *i.e.*, for the last bounces. Section 5 is devoted to the presentation and the outcomes of a non–dissipative model. This latter describes both the contact dynamic of the last bounces and the bead oscillations on the plane. We then give the derivation of an analytical expression of the period of the bead oscillations, and an integral expression of the duration of impact. The different mechanisms of energy loss occurring during a bounce are then discussed in Section 6. Finally, in Section 7, we present a dissipative numerical model which leads to an interpretation of the evolution of the restitution coefficient with the impact velocity of the bead.

2 Elementary model of the inelastic ball

A bead is dropped from a height h_0 without initial velocity. The bead falls vertically onto a perfectly smooth horizontal surface of a perfectly hard material with infinite mass, then bounces a number of times before coming to rest. During the free fall, we assume that the bead is subjected only to gravity. Besides, during each bounce, the collision is assumed instantaneous, *i.e.*, the duration of contact is zero, and inelastic, *i.e.*, a part of the kinetic energy of the bead is dissipated. The bead's velocity after a collision is therefore smaller than before the collision, and consequently the height of bounces decreases with time. Let ϵ be the ratio between the bead velocity after and before the impact. This ratio, called the restitution coefficient between the bead and the surface, is assumed constant for all bounces. As the air resistance is neglected, the bead velocity before the $n+1$th bounce corresponds to the one after the nth bounce. Thus, if v_n is the bead velocity before the nth bounce, ϵ has the following expression

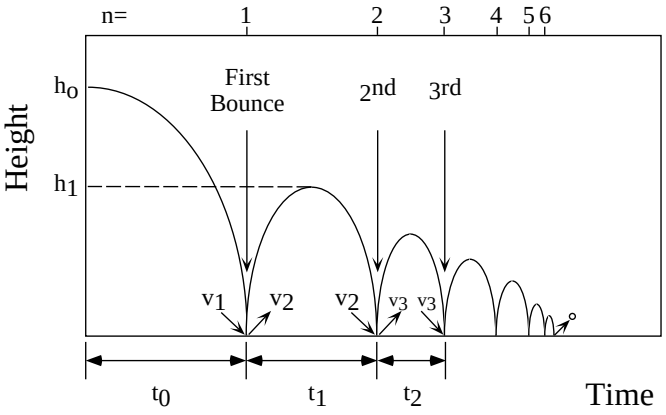

Fig. 1. Schematic representation of the first few collisions.

$$\epsilon = \frac{v_{n+1}}{v_n} \qquad (n = 1, 2, 3, \cdots) \ . \tag{1}$$

Using the notations of Figure 1, it is easy to show that the bead first strikes the surface after a time $t_0 = \sqrt{2h_0/g}$, with a velocity $v_1 = \sqrt{2h_0 g}$ where g is the acceleration of gravity. Let t_n be the time of flight of the bead between the nth and the $n+1$th bounces. Using the above assumptions, we have

$$t_n = \epsilon^{n-1} t_1 = \epsilon^n \sqrt{\frac{8h_0}{g}} \qquad (n = 1, 2, 3, \cdots) \ , \tag{2}$$

and the bead comes to rest after a time $\mathcal{T}_\infty$

$$\mathcal{T}_\infty = \sum_{n=0}^{\infty} t_n = t_0 + t_1 \times \sum_{n=1}^{\infty} \epsilon^{n-1} = \frac{1+\epsilon}{1-\epsilon}\sqrt{\frac{2h_0}{g}}, \tag{3}$$

since $\epsilon < 1$. Consequently, the bead comes to rest after an infinite number of bounces in a finite time $\mathcal{T}_\infty$.

Let ζ_n be the time passed between the release and the nth bounce, *i.e.*, $\zeta_n = \sum_{i=0}^{n} t_i$. The bouncing frequency ν_n for the nth bounce then is

$$\nu_n \equiv \frac{dn}{d\zeta_n} = \frac{1}{\ln \epsilon}(\zeta_n - \mathcal{T}_\infty)^{-1} \qquad (n = 1, 2, 3, \cdots). \tag{4}$$

Consequently, the bouncing frequency tends to infinity, a phenomenon called the "sound of singularity" in reference [20], as the bead stops, *i.e.*, as $\zeta_n \to \mathcal{T}_\infty$ or $n \to \infty$. Nevertheless, as we will show in Section 4.1 (see Fig. 3), it

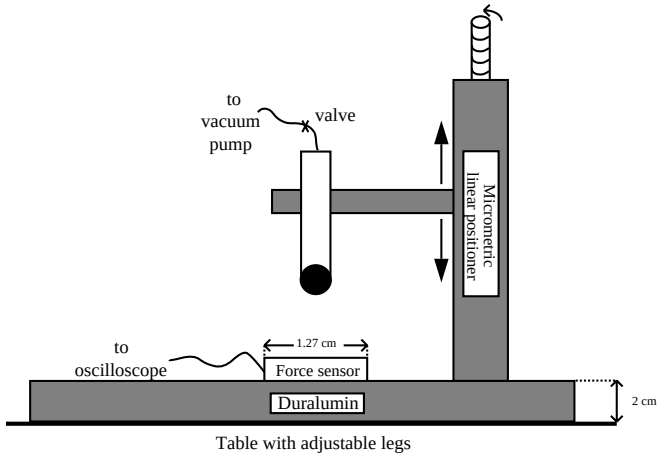

Fig. 2. Schematic diagram of the experimental setup (not to scale).

is necessary to take the finite durations of collisions into account. This elementary model is therefore unacceptable to describe the dynamic of the bead. However, it is useful to keep in mind equation (2) when analyzing experimental data for the collision times (see Sect. 4.1).

3 Experimental setup

A tungsten carbide bead, 8 mm in diameter, is suspended at the end of a vertical brass tube inside which a partial vacuum is drawn by means of a pump. The bead has a tolerance of ± 1 μm in diameter and ± 0.8 μm in sphericity. The tube is fixed on a micrometric linear positioner allowing a precise adjustment of the height of the release. A quick opening valve relieves the vacuum and releases the bead above a PCB $200B02$ piezoelectric force sensor which is screwed on a duralumin square flat plate. Each side of this latter is 30 cm long, and its thickness is 2 cm. As it is shown in Figure 2, the whole setup is fixed on a table with adjustable legs in order to ensure horizontality of the impact plane. The force sensor is connected to a digital oscilloscope performing single shot acquisition of 50 000 points with a sampling rate up to 10 ns/pt. The height of fall h_0 is 2 mm in order to avoid the plastic limit of the sensor material. For such height of fall, the air friction force on the bead motion is negligible[1]. In order to have a satisfactory resolution on the oscilloscope, *i.e.*, 5 μs/pt, only the last bounces are recorded. For all experiments the total duration of bounces is about 1.28 s and the trigger delay of the oscilloscope is 1.08 s. Only the last 0.20 s of signal are thus recorded, corresponding to about a hundred measurable bounces.

The reproducibility of measurements strongly depends of the release of the bead (*i.e.*, a fixed initial height of fall, no initial rotational and translational velocity), the tolerance in the bead diameter and sphericity, the surface roughness of the target as well as its horizontality. The principal feature of this apparatus (see also Ref. [40]) is that it releases the bead reproducibly and avoids the problems encountered with other mechanisms: Either an electromagnet (magnetization of the bead causing an induced current that distorts the piezoelectric sensor response), or a diaphragm and a screw (rotational velocity of the bead during the release). A tolerance better than ± 10 μm in diameter and ± 5 μm in sphericity allows all the bounces to occur on the sensor till the stopping of the bead. For beads with poorer tolerance than previous ones (*e.g.*, glass, nylon or polyurethane beads), it is not possible to observe the latest bounces on the sensor, even for an extremely precise adjustment of the horizontality. Indeed, during each bounce, the bead gains a very small rotational velocity due to the little differences of sphericity and diameter. This velocity becomes more and more important as the number of bounce increases, till the bead bounces outside the sensor.

[1] During the free fall in the air of a tungsten carbide bead, 8 mm in diameter, the bead should be in free fall during more than 5 s, *i.e.*, for a height of fall of the order of 150 m, in order that the bead reach its sedimentation speed.

4 Experimental results

4.1 Duration of collision

The duration of a collision is finite so that it is necessary to introduce the following variables: f_n, the time of flight of the bead between the nth and the $n+1$th bounce, d_n, the total elapsed time between the nth and the $n+1$th bounce, and τ_n the duration of the nth collision

$$d_n = \tau_n + f_n \qquad (n = 1, 2, 3, \cdots) \; . \tag{5}$$

For the elementary model of Section 2, assuming $\tau_n = 0$ whatever n, we have obviously $t_n = d_n = f_n$. Figure 3 shows the observed evolution of the natural logarithm of both f_n and d_n as a function of $n - N_0$. N_0 is the number of bounces made by the bead during the trigger delay of the oscilloscope. Till the duration of collision becomes significant, the two curves in Figure 3 are identical and are described by a linear relation between $\ln(t_n)$ and $n - N_0$ with $t_n = d_n = f_n$ since $\tau_n \ll f_n$. Taking the natural logarithm of both sides of equation (2), we identify the slope and the ordinate intercept of the straight line as, respectively, $\ln(\epsilon)$ and $\ln(\sqrt{8h_0/g}) + N_0 \ln(\epsilon)$. Experimentally, we measure the values $\epsilon = 0.974$ and $N_0 = 80$. Thus, as long as $\tau_n \ll f_n$, the elementary model in Section 2 is in agreement with experimental results since ϵ is constant.

Without taking τ_n into account, Bernstein [41,42] measures a nonlinear law between $\ln(t_n)$ and n during the first 20 bounces of a solid plastic bead dropped from a height of 1 m onto a smooth massive stone. His observations differ considerably from ours since his height of fall is 500 times greater than ours, and consequently an important amount of energy is dissipated during each impact (see Sect. 6). Note that Smith *et al.* [43] resumed Bernstein's work entirely interfacing the experiment with a computer.

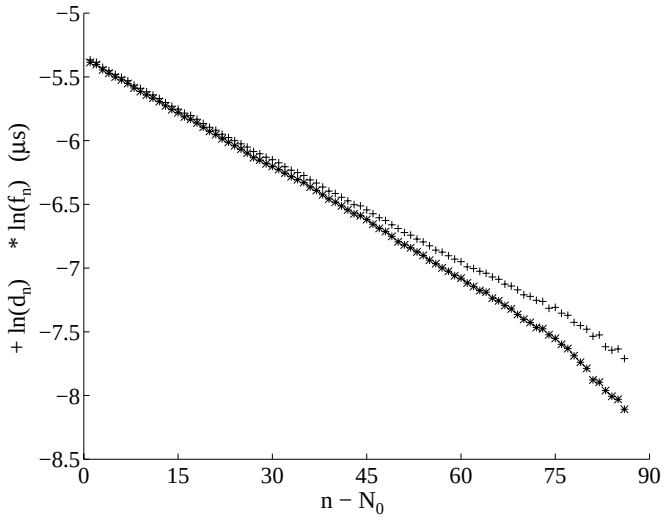

Fig. 3. Evolution of $\ln(f_n)$ $(*)$ and $\ln(d_n)$ $(+)$ as a function of $n - N_0$ for a carbide tungsten bead dropped from a height $h_0 = 2$ mm. N_0 is the number of bounces made by the bead during the trigger delay of the oscilloscope (1.08 s). The time of flight for the last two measured bounces is 301 μs $(*)$ and the total elapsed time 448 μs $(+)$.

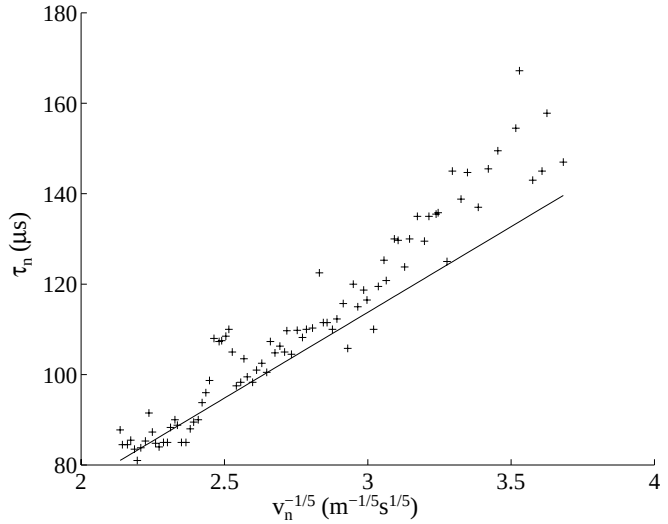

Fig. 4. Duration τ_n of the nth bounce as a function of $v_n^{-1/5}$. Crosses correspond to experimental points. The solid line corresponds to Hertz's theory $\tau = Av^{-1/5}$ with $A = 37.92 \times 10^{-6}$ m$^{1/5}$s$^{4/5}$.

Although their experimental conditions are unclear, their results seem qualitatively identical to Bernstein's ones.

Hertz's theory [39] shows that the duration of collision between a bead and a plane, with a relative velocity v, is $\tau \propto v^{-1/5}$. Thus, the smaller the velocity before the impact, the greater the duration of impact. It is clear from Figure 3 that the duration of impact increases with the number of bounces. The values of the duration of collision τ_n for each bounce are obtained from Figure 3 in accordance with equation (5). The evolution of τ_n is shown in Figure 4 as a function of $v_n^{-1/5}$. The values of v_n are extracted from the values of f_{n-1} multiplied by $g/2$. The solid line corresponds to Hertz law $\tau = Av^{-1/5}$ where A is found experimentally by means of a second oscilloscope recording the first two bounces. The measure of the duration of collision of the first impact ($\tau_1 = 52.4$ μs), knowing the height of fall ($h_0 = 2$ mm) and thus the impact velocity of the bead, gives for the value of this constant $A = 37.92 \times 10^{-6}$ m$^{1/5}$s$^{4/5}$. Figure 4 shows good agreement with Hertz's theory for $v_n^{-1/5} < 3$ m$^{-1/5}$s$^{1/5}$. Beyond 3 m$^{-1/5}$s$^{1/5}$, *i.e.*, for very small impact velocities, corresponding to the last measured bounces, the discrepancy with Hertz law is clear, despite some scattering in the experimental data: The duration of collision seems to increase much faster than according to the Hertz's law.

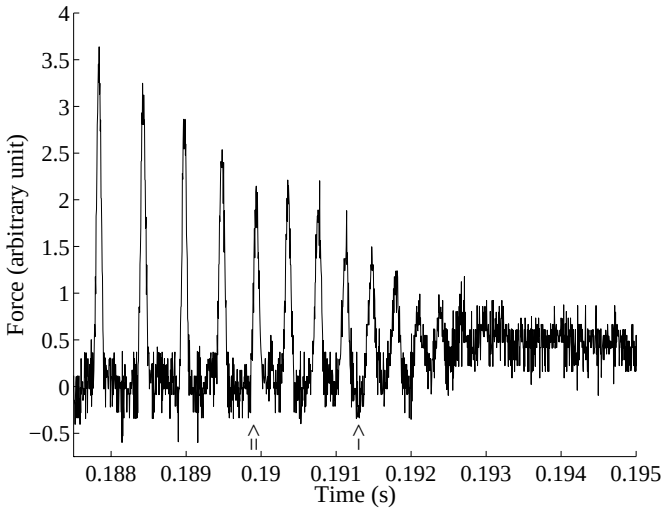

Fig. 5. Signal from the force sensor for the ultimate bounces. The double arrow indicates the location of the last measure for f_n and d_n. The single arrow indicates the time for which the bead starts to oscillate on the sensor without taking off.

4.2 Period of the bead oscillations on the sensor

The signal from the force sensor is represented in Figure 5. Only the last few bounces are shown. The double arrow indicates the location of the last measure of f_n and d_n in Figure 3, where the flight time of the last two measured bounces (300 μs) is of the order of twice the duration of the last measured bounce. Beyond, it is not possible to define the end and the beginning of two successive collisions in order to measure exactly f_n and d_n. Indeed, it is easy to find the start and the end of collisions for the first bounces because of the fast variations of the signal, whereas for the last bounces (located between the double arrow and the single arrow in Figs. 5 or 6), these variations are of the same order as the signal pseudo–period.

The single arrow indicates the end of the bouncing regime and the beginning of the oscillatory one. Indeed, as it is shown in Figure 5, beyond the single arrow the bead oscillates on the plate until the oscillation amplitude reaches the experimental noise. For times greater than

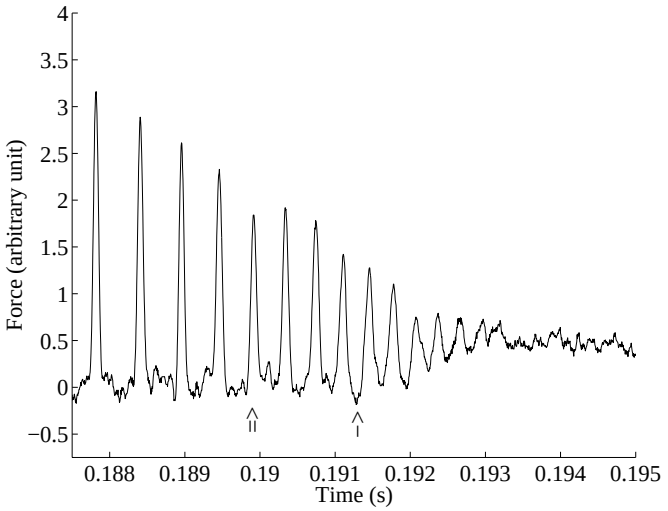

Fig. 6. Smoothing of the signal in Figure 5 by an arithmetic mean over 8 successive points (35 μs).

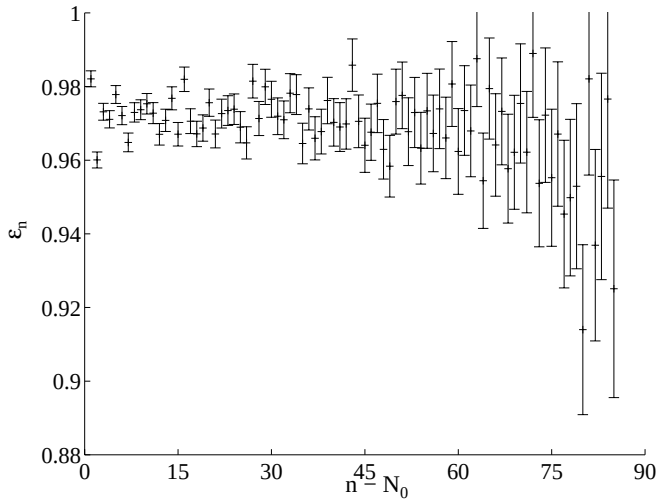

Fig. 7. Evolution of the restitution coefficient ϵ_n as a function of $n - N_0$ for a tungsten carbide bead dropped from a height $h_0 = 2$ mm. N_0 is the number of bounces made by the bead during the trigger delay of the oscilloscope (1.08 s). The error bars correspond to $\pm\Delta\epsilon_n = \pm\Delta f_{n-1}(1-\epsilon_n)/f_{n-1}$ with $\Delta f_{n-1} = 5$ μs.

the one indicated by the single arrow, the force felt by the sensor oscillates around a constant and non–zero mean value. This comes from the fact that the sensor feels the weight of the bead: The bead no longer takes off but "spends all its time" oscillating on the sensor, before coming to rest.

After the last bounce, the impact velocity is so small that the bead has not the time to end its quasi–elastic loading and unloading cycle before feeling again gravity in a significant way, so that the bead does not take off from the sensor.

In order to measure the period of the bead oscillations, the signal recorded by the oscilloscope and shown partially in Figure 5 is transferred to a computer. To maximize the signal to noise ratio, each point of the smoothed curve in Figure 6 has been redefined from a point of the original signal, at the same abscissa, by an arithmetic mean over the 4 points before and the 4 points after. Then, we measure the typical frequency of the smoothed curve in Figure 6 for the last five oscillations, which leads to the period of the bead oscillations

$$T_{exp} = 297\ \mu\text{s} \pm 20\ \mu\text{s}. \qquad (6)$$

4.3 Restitution coefficient

For a given collision, the restitution coefficient is defined as the ratio of the bead's velocity after and before the impact. The values of the restitution coefficient are extracted from those of the time of flight between two successive bounces. Using the notations in Sections 2 and 4.1, and the fact that the air resistance is negligible, the restitution coefficient for the nth impact is

$$\epsilon_n = \frac{v_{n+1}}{v_n} = \frac{f_n}{f_{n-1}} \qquad (n = 1, 2, 3, \cdots)\ . \qquad (7)$$

Figure 7 shows the evolution of the restitution coefficient ϵ_n as a function of the bounce's number for $n > N_0$. For the first $N_0 = 80$ bounces (not represented here), the restitution coefficient is found to be essentially constant and equal on average to 0.97. For $n > N_0$, the value of the restitution coefficient, for each bounce, is obtained from the last 200 ms signal recorded from the force sensor according to equation (7). Unlike the assumption of the elementary model in Section 2, ϵ_n is not constant for all bounces but fluctuates around the mean value 0.97 before decreasing for the last bounces. Thus, the restitution coefficient is not only a property of the materials in collision, but also a characterization of the dynamics of the collision, and of the actual way in which energy dissipation occurs. The different mechanisms of energy dissipation occurring during a bounce are discussed in Section 6. Except for the very last bounces, the velocity loss is of the order of 3% corresponding to a combined energy loss effect in the form of elastic waves, flexural vibrations of the plate and viscoelastic behavior of the bead and the target (see Sect. 6). The fluctuations around this mean value are due to the fact that the restitution coefficient is very sensitive to the slightest surface imperfections of the target since the contact radius is very small (of the order of 10^{-4} m to 10^{-6} m when the impact velocity varies from 10^{-1} m/s to 10^{-5} m/s). Although the errors on the measurement of ϵ_n are more and more important as the impact velocity decreases, ϵ_n seems to decrease for the very last measured bounces. Since the dissipated energy both in the form of elastic waves and in the form of viscoelastic or flexural vibrations of the target has to decrease when the velocity decreases (see Sect. 6), the decrease of ϵ_n in Figure 7 could be an indication of the appearance of a new mechanism of dissipation. However, as it will be shown in Section 7, it will be nothing of the sort.

5 Conservative model

In this section, we show that the nonlinear Hertz interaction cannot describe the last bounces and the bead oscillations on the sensor reported above. To this end, the Hertz's contact law will be modified, taking gravity into account during the interaction between the bead and the sensor. Obviously, we will not be able to describe the dissipative phenomena intrinsic to the experiment that will be considered in Section 7.

Let x be the distance between the bead and the ground[2] located on a vertical downward axis with the ground surface as origin. Consequently, an interpenetration between the bead and the surface will correspond to a positive displacement x whereas the bead detachment from the surface will correspond to a negative displacement. If the dissipation is neglected, the bead is subjected to its weight whatever the sign of x and to the Hertz's interaction with the ground when $x > 0$. The bead motion is governed by the following equation

$$m\frac{d^2x}{dt^2} = mg - k|x|^{3/2}H(x), \tag{8}$$

where

$$H(x) = \begin{cases} 1 \text{ if } \ x > 0, \\ 0 \text{ otherwise,} \end{cases}$$

with $m = 4 \times 10^{-3}$ kg the mass of the tungsten carbide bead and $g = 9.81$ m/s^2 the acceleration of gravity. The constant k is the coefficient of the Hertz's law for a sphere–plane contact and reads [39]

$$k = \frac{4}{3}\sqrt{R}\left(\frac{1-\nu_s^2}{E_s} + \frac{1-\nu_c^2}{E_c}\right)^{-1}, \tag{9}$$

where E_c and ν_c are, respectively, the Young's modulus and the Poisson's ratio of the stainless steel coated sensor, E_s and ν_s being the corresponding quantities for a tungsten carbide bead of radius R. Using the properties of tungsten carbide ($\nu_s = 0.22$ and $E_s = 53.4 \times 10^{10}$ N/m^2) [44] and $R = 4$ mm, a good estimate of k is obtained if we let $\nu_c = 0.276$ and $E_c = 21.6 \times 10^{10}$ N/m^2, as for plain stainless steel [44]; the result is

$$k = 1.392 \times 10^{10} \text{ kg m}^{1/2}\text{s}^{-2}. \tag{10}$$

We just describe the contact between the bead and the ground, *i.e.*, $x > 0$. Equation (8) becomes

$$\frac{d^2x}{dt^2} = g - \frac{k}{m}x^{3/2}. \tag{11}$$

The weight of the bead may be neglected during its interaction with the ground if the second term of the left hand–side of equation (11) is greater than g, *i.e.*, for x such that

$$x \gg \left(\frac{mg}{k}\right)^{2/3} \sim 10^{-8} \text{ m}. \tag{12}$$

[2] In practice, the "ground" corresponds to the top of the force sensor. We will keep this designation afterwards.

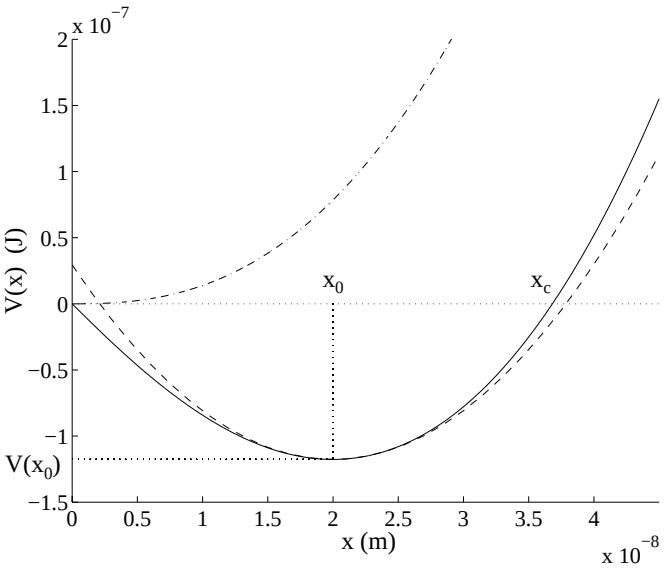

Fig. 8. Shape of the potential $V(x) = -gx + \frac{2k}{5m}x^{5/2} + C$, with $C = 0$, as a function of the interpenetration distance x (solid line). x_0 is the abscissa of the minimum of $V(x)$. x_c is the critical maximal interpenetration such that for $x_{max} > x_c$ the bead separates from the ground whereas for $x_{max} \leq x_c$ the bead oscillates on the ground around x_0. Shape of the potential $V(x)$ around x_0: $V(x) \approx V(x_0) + \frac{3k}{4m}x_0^{1/2}(x-x_0)^2$ (dashed line) and of the Hertz's potential $V^*(x) = \frac{2k}{5m}x^{5/2} + C$ with $C = 0$ (dot–dashed line) as a function of x.

When the bead is dropped from a height of the order of millimeter, the maximal distance of interpenetration is of the order of micrometer. The effects of gravity during the interaction are therefore negligible for the first bounces. However, at the end of the bounces, the impact velocities are very small and the bead can embed on a distance of the order of 10^{-8} m; the bounces dynamics is then modified in a significant way by gravity.

Equation (11) can be put in the form of an equation describing the motion of a point mass in a potential $V(x)$

$$\frac{d^2x}{dt^2} = -\frac{dV}{dx} \quad \text{where} \quad V(x) = -gx + \frac{2k}{5m}x^{5/2} + C, \tag{13}$$

with C a constant of integration determined by the initial conditions. This potential energy corresponds to the sum of elastic energy and gravitational potential energy. The dynamics of the system is governed by the competition between those two energies. The shape of this potential is shown in Figure 8. The abscissa x_0 of the minimum of the potential is

$$x_0 = \left(\frac{mg}{k}\right)^{2/3} \simeq 2 \times 10^{-8} \text{ m}, \tag{14}$$

and the intercept of $V(x)$ with the x–axis, for $C = 0$, is

$$x_c = \left(\frac{5mg}{2k}\right)^{2/3} \simeq 3.68 \times 10^{-8} \text{ m}. \tag{15}$$

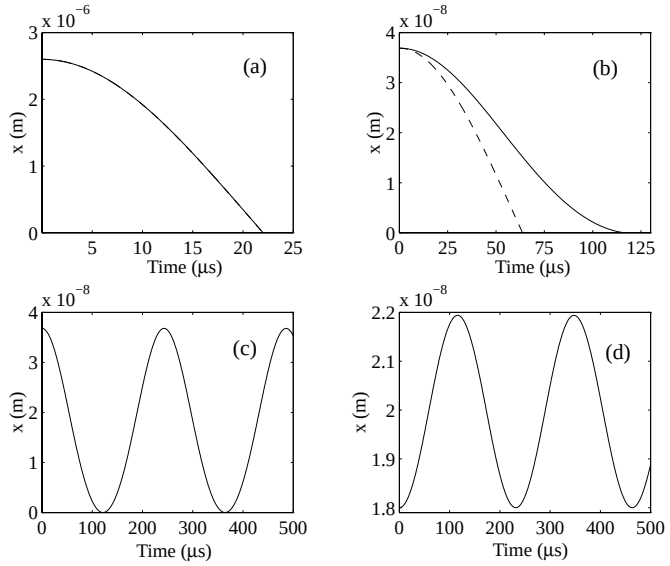

Fig. 9. Interpenetration x as a function of time for different values of x_{max}: (a) $x_{max} = 2.6 \times 10^{-6}$ m $\gg x_c$; (b) $x_{max} = 3.69 \times 10^{-8}$ m $> x_c$; (c) $x_{max} = 3.68 \times 10^{-8}$ m $= x_c$; (d) $x_{max} = 1.8 \times 10^{-8}$ m $< x_c$. The dashed line in Figures (a) and (b) are obtained from Hertz's law where gravity is neglected. Solid lines correspond to the numerical integration of equation (11). Notice that in Figure (a) both curves are identical. The oscillation periods in Figures (c) and (d) are, respectively, 242 and 231 μs. In Figures (a) and (b), the calculations diverge when the bead separates from the ground ($x < 0$) whereas those in Figures (c) and (d) are stopped after 500 μs.

During the contact between the bead and the ground, the bead undergoes its loading cycle from $x = 0$ up to a maximal distance of interpenetration x_{max} where its velocity vanishes. At this instant, the bead has only potential energy. If this total energy is large enough ($V(x_{max}) > 0$), *i.e.*, if x_{max} is large enough ($x_{max} > x_c$), the bead will have stored enough elastic potential energy to be able to make completely its unloading cycle and then to take off the ground. On the other hand, if $x_{max} \leq x_c$, the elastic potential energy stored at the end of the loading cycle will be too weak ($V(x_{max}) \leq 0$) to allow the bead to complete its unloading cycle. In that case, the motion of the bead is oscillatory, with a constant amplitude since we assume in this model that there is no energy dissipation.

The previous results, based on a simple study of the potential $V(x)$, are confirmed by the numerical integration of equation (11). At $t = 0$, we assume that the bead has ended the loading cycle and is located in $x(0) = x_{max}$ where its velocity is $\dot{x}(0) = 0$. With those initial conditions, we can study the bead motion for different values of x_{max}.

Figure 9 shows the evolution of the interpenetration x as a function of time, during the unloading cycle, for different values of x_{max}. When the bead is dropped from a height of 2 mm, the maximal interpenetration is $x_{max} = 2.6$ μm; and consequently gravity is negligible compared to the elastic force (see Eq. (12)). The unloading cycle is governed by the Hertz's law, as it is shown in Figure 9a, until the bead takes off the ground after a contact of 42.8 μs. Figure 9b shows the evolution of x for a contact time large compared to the previous one, *i.e.*, for x_{max} so small that it is necessary to take into account gravity during the unloading cycle. However, x_{max} is slightly greater than x_c, which allows the bead to have enough stored elastic energy to be able to take off the ground. The discrepancy between the dashed line in Figure 9b, solution of the standard Hertz's law, and the solid line, solution of equation (11), shows the importance of gravity during the interaction. For $x_{max} \leq x_c$, the bead has no longer enough elastic energy to take off the ground (see Fig. 8) and oscillates infinitely on the ground, since the system is conservative (see Figs. 9c–d).

5.1 Influence of gravity on the contact time

By multiplying equation (11) by (dx/dt) and integrating over time t, we obtain

$$\frac{1}{2}\left(\frac{dx}{dt}\right)^2 = gx - \frac{2k}{5m}x^{5/2} + C, \tag{16}$$

where the integration constant C is determined by three independent conditions: First, at $t = 0$, $x(0) = 0$ and $(dx/dt)|_{t=0} = v_{imp}$ and, on the other hand the bead velocity is zero when $x = x_{max}$. Thus,

$$C = \frac{1}{2}v_{imp}^2 = -gx_{max} + \frac{2k}{5m}x_{max}^{5/2}. \tag{17}$$

The relation between the bead velocity v_{imp} just before the impact and the maximal interpenetration made during this impact is then

$$v_{imp} = \sqrt{\frac{4k}{5m}x_{max}^{5/2} - 2gx_{max}}, \quad \text{with} \quad x_{max} \geq x_c, \tag{18}$$

The second term under the square root is the correction to Hertz's law due to the effect of gravity. Indeed, with $g = 0$ in equation (18), we find again the standard result for the interpenetration x_{max}^* derived from the Hertz's law.

We may integrate equation (16); since there is no dissipation, the duration of collision is twice the time spent by the bead to go from $x = 0$ to $x = x_{max}$, so that the total contact time reads

$$\tau = 2\int_0^{x_{max}} \frac{dx}{\sqrt{v_{imp}^2 + 2gx - \frac{4k}{5m}x^{5/2}}}. \tag{19}$$

With $\nu = x/x_{max}$, equation (19) becomes

$$\tau = 2\frac{x_{max}}{v_{imp}}\int_0^1 \frac{d\nu}{\sqrt{1 + a\nu - b\nu^{5/2}}}, \tag{20}$$

where a and b are functions of x_{max} such that

$$\frac{1}{a} = \frac{2k}{5mg}x_{max}^{3/2} - 1 \quad , \quad \frac{1}{b} = 1 - \frac{5mg}{2kx_{max}^{3/2}}\,. \tag{21}$$

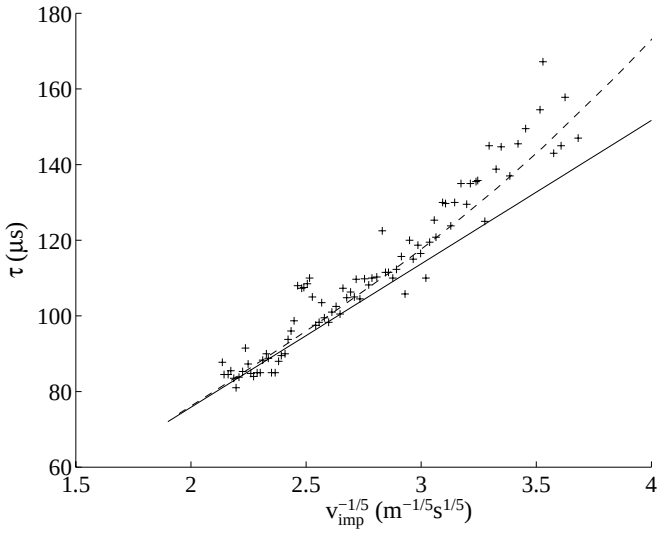

Fig. 10. Evolution of the duration τ of collision as a function of $v_{imp}^{-1/5}$: Numerical integration of equation (20), with $k = k_{exp}$, for different values of x_{max} (dashed line); power law $\tau^* = 2,94\left(\frac{5m}{4k_{exp}}\right)^{2/5} {v_{imp}}^{-1/5}$ derived from Hertz's law (solid line identical to the one in Fig. 4). Crosses are the experimental points.

The duration of impact τ is a function of one single variable x_{max} or v_{imp}, since both are linked by equation (18). Equation (20) may be compared with the duration of impact derived from the Hertz's law, which reads

$$\tau^* = 2\frac{x^*_{max}}{v_{imp}} \int_0^1 \frac{d\nu}{\sqrt{1-\nu^{5/2}}} \simeq 2.94\frac{x^*_{max}}{v_{imp}} \cdot \qquad (22)$$

The integral in equation (20) has no analytical expression, but may be calculated by numerical integration. In order to compare quantitatively the experimental results of the duration of collision (Fig. 4) with the numerical ones, it will be necessary to change the value of the constant k. Indeed, the coefficient k of the Hertz's law has been calculated for a contact between a massive tungsten carbide sphere and a massive stainless steel plane. It is obvious that the elastic parameters of the force sensor, coated by stainless steel, are not the same as the ones of a massive stainless steel material. And the ones of a tungsten carbide bead, which is probably an alloy of tungsten carbide and cobalt, are not exactly the same as the ones of a massive tungsten carbide material.

However, an experimental value k_{exp} can be extracted from the duration of collision of the first bounce. Since the duration of a collision is obtained by the Hertz's law, in inserting equation (18) with $g = 0$ into equation (22), it is easy to find an experimental value of k, knowing the measure of the duration of collision of the first bounce (see Sect. 4.1) and the height of the free fall: $k_{exp} = 8.386 \times 10^9$ kg m$^{1/2}$s^{-2}. Notice that this value is considerably smaller than the one of equation (10).

The dashed line in Figure 10 shows the evolution of τ, calculated by numerical integration of equation (20), with $k = k_{exp}$, for different values of x_{max}, as a function of ${v_{imp}}^{-1/5}$. The experimental results (crosses) are qualitatively and quantitatively similar to the ones of the Hertz's model modified by gravity (dashed line): The duration of collision increases much faster than the prediction of the Hertz's theory. The gravity causes the bead to spent a longer time on the sensor. This behavior comes from the fact that at a fixed impact velocity, we have $x_{max} > x^*_{max}$. Indeed, gravity is opposed to the elastic force.

This difference between the two models diverges when $v_{imp} \to 0$, *i.e.*, using equation (15) and equation (18), when $x_{max} \to x_c$ for the Hertz's model modified by gravity whereas $x^*_{max} \to 0$ for the pure Hertz's model. This means that when a bead is put without velocity on the ground, the bead is slightly compressed on a maximal distance x_c when gravity is taken into account, whereas no deformation occurs with the pure Hertz's model. Thus, at $v_{imp} = 0$, *i.e.*, for $x_{max} = x_c$, the influence of gravity during the interaction causes the bead to oscillate infinitely on the plane surface (see Fig. 9c).

Obviously, experimentally, the value $v_{imp} = 0$ is never reached and thus x_{max} cannot be less than or equal to x_c and consequently, the bead oscillations on the sensor should be not observable. However, although the impact velocity for the last bounces is not exactly equal to zero, the dissipation during the contact allows the bead to reach a value of x_{max} less than x_c. The oscillatory motion is then also damped because of dissipative effects.

5.2 Period of the bead's oscillations

The simulations in Figure 9 have shown that the effect of gravity dominate the elastic one for $x_{max} \leq x_c$; below this critical value the bead oscillates with a constant period. The difference with the experimental result (the decay of the amplitudes of oscillations) is due to the absence of dissipation in the model. In this section, an expression of the period of the bead oscillations is derived and compared to the experimental value (T_{exp}) and the numerical one (Figs. 9c–d).

Dimensional analysis of equations (16) and (17) gives the general expression of the period of oscillations

$$T = B\left(\frac{m}{kg^{1/2}}\right)^{1/3} F\left[\frac{x_{max}}{x_0}\right], \quad \text{with} \quad x_{max} \leq x_c, \quad (23)$$

where B is a numerical constant and $F[\cdot]$ an unknown function. Note that this period depends on the maximal amplitude of the oscillations x_{max}.

First, assume that the amplitude of the oscillations are small, *i.e.*, $x_{max} \simeq x_0$, and F is a constant. For $x_{max} \leq x_c$, the system oscillates around x_0. We may develop around x_0 the potential $V(x)$ of equation (13) as displayed by the dashed line in Figure 8. Identifying the bead motion in the vicinity of x_0 with an harmonic oscillator, and using equation (14), we obtain the expression of the period of the bead oscillation around x_0

$$T\big|_{x_{max} \simeq x_0} = 2\pi\sqrt{\frac{2}{3}}\left(\frac{m}{kg^{1/2}}\right)^{1/3}. \qquad (24)$$

In order to compare the theoretical value to the experimental one, T is calculated from equation (24) with $k = k_{exp}$ which leads to

$$T\big|_{x_{max}\simeq x_0} \simeq 274\ \mu\text{s}, \tag{25}$$

which is in fair agreement with the experimental result (Eq. (6)). Moreover, we can compare the numerical value $T_{num} \simeq 231\ \mu$s found by the simulation for x_{max} close to x_0 (see Fig. 9d), with k as in equation (10). Equation (24) with k as in equation (10) then leads to $T \simeq 231\ \mu$s which is in very good agreement with T_{num}.

For large amplitude oscillations, the period is given by equation (19) with $v_{imp} = 0$ and $x_{max} = x_c$, setting $\nu = x_{max}/x_c$, such that

$$\begin{aligned} T\big|_{x_{max}=x_c} &= 2\sqrt{2}\left(\frac{5}{3}\right)^{1/3}\left(\frac{m}{kg^{1/2}}\right)^{1/3}\int_0^1 \frac{d\nu}{\sqrt{1-\nu^3}} \\ &\simeq 5.38\left(\frac{m}{kg^{1/2}}\right)^{1/3}. \end{aligned} \tag{26}$$

The theoretical value of the period of large amplitude oscillations is calculated from equation (26) with $k = k_{exp}$ and leads to

$$T\big|_{x_{max}=x_c} \simeq 287\ \mu\text{s}, \tag{27}$$

which is in good agreement with the experimental value of (6). Moreover, we can compare the numerical value $T_{num} \simeq 242\ \mu$s found by the simulation for x_{max} close to x_c (see Fig. 9c), with k as in equation (10). Equation (26) with k as in equation (10) then leads to $T \simeq 243\ \mu$s.

6 Mechanisms of energy loss during a collision

During an ideal bounce, *i.e.*, an elastic collision, all the kinetic energy of the bead is converted into elastic strain energy during the deformation process, and then reconverted into kinetic energy when the bead takes off. In pratice, some energy is always lost during an loading and unloading cycle. This energy loss, comparable to an effective dissipation, comes mainly from three mechanisms:

1. Energy loss due to the vibration radiated in the target (surface and volumic waves and vibrational modes) and the residual vibrations stored in the bead after the collision,
2. Energy loss due to a plastic deformation of the bead or/and the target,
3. Energy dissipation due to the viscoelastic properties of the bead and the target.

However, for our experiments, the first two mechanisms are almost negligible and independent of the impact velocity:

- *Dissipated energy in the form of elastic waves*
  This has been studied theoretically by Hunter [29] and Reed [30]. They showed that the dissipated energy into the target in the form of elastic waves decreases with decreasing impact velocity. Reed's theory [30] has been confirmed experimentally [30–32] and predicts, for our experiments, a variation of the restitution coefficient due to this form of energy losses about 0.7% if the impact velocity ranges from 0.2 to 0 m/s.
- *Dissipated energy in the form of vibrational modes of the target*
  The restitution coefficient is independent of the finite extent of the target if the plate is thicker than a few diameters of the impacting bead [31–34]. If this condition is not fulfilled, the restitution coefficient ϵ decreases when the impact velocity increases. Experimentally, a preliminary study with plates of different thicknesses (5, 10 and 15 mm) has shown that ϵ decreases when the impact velocity increases. The thickness we have finally chosen (20 mm) leads to a restitution coefficient which is constant and independent of the impact velocity. For our experiments, Zener's theory [34] predicts a variation of the restitution coefficient due to the energy losses in form of flexural modes of the target (which are the most important ones for a plate [31]) lower than 2.5% if the impact velocity ranges from 0.2 to 0 m/s.
- *Energy loss due to plastic deformation*
  If a critical impact velocity is exceeded, the impact causes plastic deformation and some energy is lost to produce the plastic indentation. This critical velocity is very small for most impacts between metallic bodies, *i.e.*, of the order of 0.1 m/s [45]. At significantly higher velocities fully plastic deformation occurs, and when this stage is reached, *i.e.*, of the order of 5 m/s [45], the experiments of references [27,28,35] confirm the theory [26,35] indicating a restitution coefficient proportional to the power $-1/4$ of the impact velocity. When impacts lie between the critical velocity for plastic indentation and the fully plastic deformation velocity, the restitution coefficient is nearly constant for the lower velocities and gradually falls at higher velocities [26,33,36,37,46]. Our initial impact velocity being less than 0.2 m/s, all the bounces may be almost considered without plastic indentation.

Consequently, within our experimental conditions, the only important dissipative mechanism is the viscoelastic one.

7 Viscoelastic dissipative model

The conservative model of Section 5 describes in a satisfactory way the bounces of the bead as well as the bead oscillations on the sensor. However, in practice, during a quasi–elastic binary collision, a very small amount of energy is always lost by the system (see Sect. 6). In order to take these dissipative phenomena into account, a dissipative force F_{diss} is inserted into equation (8)

of the conservative model

$$m\frac{d^2x}{dt^2} = mg - k|x|^{3/2}H(x) - F_{diss}H(x) \qquad (28)$$

where $H(x)$ is as defined previously.

We have seen in Section 6 that the energy losses due to the vibrations radiated in the target and the bead or to the creation of plastic deformation are almost negligible and independent of the impact velocity. Thus, subsequently, we will only take into account the viscoelastic mechanism of dissipation and F_{diss} then reads

$$F_{diss} = \mu\dot{x}|x|^{\gamma}, \qquad (29)$$

where γ is a real number characterizing the linear ($\gamma = 0$) or nonlinear ($\gamma \neq 0$) nature of the viscoelastic force, and μ is a dissipation coefficient.

The viscous contact force $F = -k|x|^{3/2} - \mu\dot{x}|x|^{\gamma}$ of equation (28) has been used in numerical simulations with $\gamma = 0$ [47,48] and $\gamma = 1/4$ [49], in order to describe the interaction law between grains in a granular medium. A comparative study of the properties of these viscoelastic interaction laws, frequently used in numerical simulations, have been made recently [50,51]. From a theoretical point of view, taking only the viscoelastic dissipative effects into account, Kuwabara and Kono [38], and others [52,53] generalize the Hertz's arguments and derive an expression of the contact force between two interacting viscoelastic bodies. In a quasi–static limit, they found a dissipative force of the form of equation (29) with $\gamma = 1/2$.

For a collision between a sphere and a plane, we can generalize the Kuwabara and Kono's work [38] for $\gamma = 1/2$ to any value of γ to derive an expression of the restitution coefficient as a function of the impact velocity. This expression will be valid for an interaction law described by equation (28) for $x > 0$, in the weakly dissipative regime, without the gravity term and with a viscoelastic force given by equation (29). In the limit $\epsilon \to 1$, it is possible to show [54] that

$$\epsilon = 1 - \frac{4}{5}\mathcal{B}\left[\frac{3}{2}\,,\,\frac{2}{5}(\gamma+1)\right]\varphi \qquad \forall\gamma > -1, \qquad (30)$$

with

$$\varphi = \frac{\mu}{m}\left(\frac{5m}{4k}\right)^{2(\gamma+1)/5} v_{imp}^{(4\gamma-1)/5}, \qquad (31)$$

and $\mathcal{B}[y,z]$ a Beta function[3] where y and z must be real numbers with positive real parts. This general expression of ϵ confirms estimates for the velocity dependence of the restitution coefficient reported by Luding *et al.* [51] and leads for $\gamma = 1/2$ to the same expression as the one derived by Kuwabara and Kono (see Eqs. (9, 12) in Ref. [38]).

The evolution of ϵ from equations (30) and (31) is shown in Figure 11 as a function of v_{imp} for $\gamma = 0$, 1/4 and 1/2. For each value of γ, the dissipative parameter μ is chosen to get the best fit of the experimental results. When the impact velocities are large enough, so that gravity is negligible, the results derived from equations (30) and (31), *i.e.*, $1 - \epsilon \propto v_{imp}^{(4\gamma-1)/5}$, should be in agreement with the experimental ones. Experimentally, for such velocities, ϵ is constant in average and independent of v_{imp} (see crosses in Fig. 11), the fluctuations of the experimental data around this mean value being due to the slight surface imperfections of the bodies in contact (see Sect. 4.3). This implies $\gamma = 1/4$. Obviously, when gravity is non negligible, *i.e.*, at low impact velocities, equations (30) and (31) are no longer valid and consequently, we have disagreement with the experimental data (see lines in Fig. 11). Thus, we have to look for which value of γ, (29) best describes the experimental results at low impact velocity. This is the aim of the next two sections. Only three values of γ will be considered: $\gamma = 0$ for simplicity (linear model), $\gamma = 1/4$ since this model leads to $\epsilon \propto (v_{imp})^0$ which is correct at high impact velocity, and $\gamma = 1/2$ corresponding to the theoretical model of reference [38].

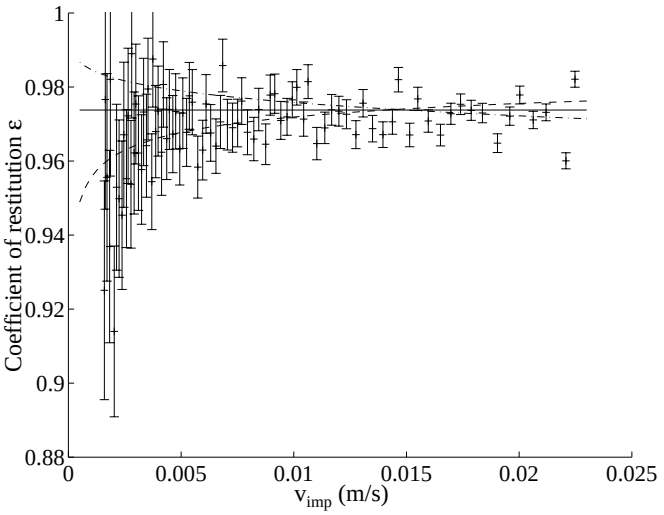

Fig. 11. Coefficient of restitution ϵ as a function of v_{imp}. Crosses correspond to experimental points. Lines correspond to theoretical solutions of equations (30) and (31): $\gamma = 0$ with $\mu/m = 530$ s^{-1} (dashed line); $\gamma = 1/2$ with $\mu/m = 1.3 \times 10^6$ m$^{-1/2}$s^{-1} (dot–dashed line) and $\gamma = 1/4$ with $\mu/m = 2.7 \times 10^4$ m$^{-1/4}$s^{-1} (solid line). In all cases, $k/m = k_{exp}/m = 2.092 \times 10^{12}$ m$^{1/2}$s^{-2}.

7.1 Phenomenological viscoelastic models ($\gamma = 0$ and $\gamma = 1/4$)

A fourth order Runge–Kutta method is used for numerically solving the nonlinear equation (28) for $\gamma = 0$ or $\gamma = 1/4$. At $t = 0$, the bead hits the plane with an impact

[3] See equation (8.380.11) in reference [55] for a definition of the Beta function.

velocity v_{imp}. The initial conditions of the problem are thus $x(t=0)=0$ and $\dot{x}(t=0)=v_{imp}$. The integration time step is much less than the typical impact time[4] of a sphere and a plane: The duration of the first bounce is 52.4 μs and the time step 0.5 μs. The numerical integration is stopped when the interpenetration x becomes negative, *i.e.*, at the end of the interaction between the bead and the plane, determining then the duration τ of the collision. The velocity of the bead v_f at the end of the collision is given by $\dot{x}(t=\tau)$ and the value of the restitution coefficient by v_f/v_{imp}. Repeating this procedure for various values of the impact velocity v_{imp}, we have then access to the evolution of the restitution coefficient as a function of v_{imp} for a choice of the dissipative parameter μ (see the dashed curve for $\gamma=0$ and the solid one for $\gamma=1/4$ in Fig. 12). For both cases, when gravity is no longer negligible, we observe an increasing energy dissipation with decreasing velocity, a trend identical to the one observed experimentally.

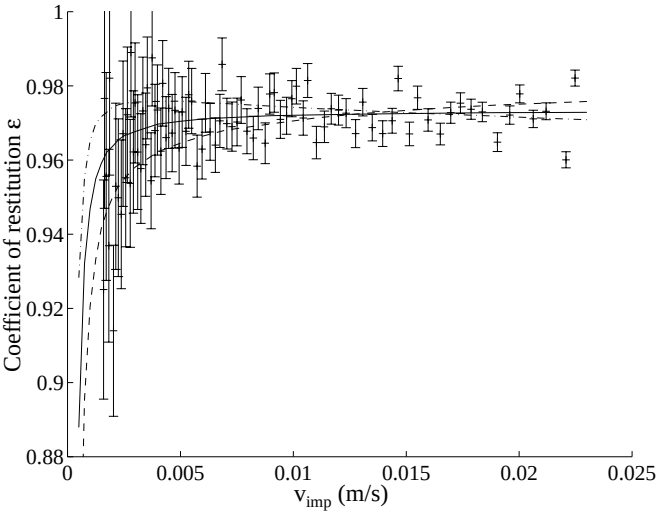

Fig. 12. Coefficient of restitution ϵ as a function of v_{imp}. Crosses correspond to experimental points. Lines correspond to numerical simulations: $\gamma=0$ with $\mu/m=530$ s^{-1} (dashed line); $\gamma=1/2$ with $\mu/m=1.3\times10^6$ m$^{-1/2}$s^{-1} (dot–dashed line) and $\gamma=1/4$ with $\mu/m=2.7\times10^4$ m$^{-1/4}$s^{-1} (solid line). For all simulations: $k/m=k_{exp}/m=2.092\times10^{12}$ m$^{1/2}$s^{-2} and v_{imp} varies from 2.3×10^{-2} to 5×10^{-4} m/s with a 2.5×10^{-4} m/s step.

7.2 Theoretical viscoelastic model ($\gamma=1/2$)

Although the previous model with $\gamma=1/4$ is in fair agreement with the experimental results both at high and low velocities, the dissipative force (29) with $\gamma=1/4$ has been inserted in a phenomenologic way in equation (28). As said above, the generalization of Hertz's theory of elastic contact leads

$$F=-k|x|^{3/2}-\mu\dot{x}|x|^{1/2} \tag{32}$$

where k is the coefficient of the Hertz's law for a sphere–plane contact (see Eq. (9)) and μ the dissipation coefficient such as $\mu=\frac{3}{2}kD$. D is a function of the elastic coefficients of the sphere (E_s and ν_s) and the plane (E_p and ν_p) materials as well as of the viscous coefficients, associated respectively with volume deformation and shear, of the sphere (respectively ξ_s and η_s) and the plane (respectively ξ_p and η_p) materials [38,52,53].

The values of ξ and η, representing viscosities in a solid, can be obtained experimentally from the measurements of the velocities and the attenuation constants of the longitudinal and transverse acoustic waves [38,39]. However, the values of those parameters at a frequency of the order of 10 kHz, corresponding to the duration of the collision, are not available in the literature [38]. We will thus take D as an adjustable parameter.

Notice that the expression of the contact force in equation (32) is derived in the quasi–static regime, *i.e.*, when the characteristic velocity v_{imp} of the problem is much less than the speed of sound in both the sphere and plane materials [53]. This quasi–static approximation is valid since the maximum impact velocity is $v_{imp}=0.2$ m/s whereas the speeds of sound in tungsten carbide and stainless steel are respectively about 6000 and 5000 m/s [44]. When gravity is negligible during the interaction, and for ϵ close to one, the restitution coefficient depends on the power 1/5 of the impact velocity as shown in equations (30) and (31) with $\gamma=1/2$. This velocity dependence of the restitution coefficient is in fair agreement with a collision experiment [38] between two identical spheres, for different materials and impact velocities ($0.5<v_{imp}<5$ m/s). These velocities are small enough to avoid any dissipation due to fully plastic deformations but great enough to cause plastic deformations (see Sect. 6). A set of experiments [11–13] deals with the collision of a water–ice sphere with a stationary flat ice brick, at very low impact velocities ($0.015<v_{imp}<5.1$ cm/s). For this range of velocity, the restitution coefficient tends towards 1 when the impact velocity tends towards zero. These experiments are fairly well described by the viscoelastic theory with $\gamma=1/2$ for frost covered ice spheres [52,53]. However, in these experiments, collisions between a disk pendulum and a flat surface are studied [11–13]. Because of this geometry, gravity effects are negligible during the interaction even at very low impact velocities but problems associated with effective mass arise [56].

When gravity effects are no longer negligible, *i.e.*, when the impact velocity becomes very small, the evolution of ϵ given by equation (30) with $\gamma=1/2$ is no longer valid. The evolution in presence of gravity is then determined numerically. Using a dissipative force (29) with $\gamma=1/2$, we integrate numerically the equation (28) proceeding in the same way as in Section 7.1. The evolution of the restitution coefficient is then plotted as a function of the impact velocity for a choice of the dissipation coefficient μ (see

[4] This impact time is the smallest time scale appearing in the system, since equation (28) makes sense in the quasi–static limit where acoustic wave propagation within a bead is neglected.

the curve in dot–dashed line in Fig. 12). The restitution coefficient decreases in a significant way at very low impact velocity. This means that the system dissipates more energy since the bead's weight is taken into account during the interaction.

In conclusion, at fairly low impact velocity, the energy dissipated by the bead is almost due to a viscoelastic mechanism and a small part to elastic waves emission and flexural vibrations. At lower impact velocity, the strong decrease of the restitution coefficient when $v_{imp} \to 0$ does not come from a new mechanism of dissipation, but from the fact that the system dissipates the energy in a different way. Indeed, when the gravity force is prominent compared to the elastic force, the system dissipates more energy than when the gravity force is negligible during the interaction. This is clear from Figure 12 whatever the choice of the dissipative viscoelastic force.

8 Conclusion

An experimental study of the behavior of one bead bouncing repeatedly off a stationary flat surface has been done. We have observed that when the duration of a collision becomes of the order of the flight time between two successive bounces, the bead no longer bounces but oscillates on the surface with a characteristic period. An analytical expression of this period has been derived and is consistent with the experimental results. We have also measured the duration of impact and the restitution coefficient for each bounce. The restitution coefficient has been found to be essentially constant and close to 1 during almost all bounces before decreasing to zero when the impact velocity tends towards zero. Moreover, at these very small impact velocities, the value of the duration of impact has been found to be longer than the prediction of Hertz's theory [39]. An integral expression of the duration of impact has been also derived.

A non–dissipative model, based on Hertz's interaction between the bead and the plane, gives results in fair agreement with the experiments when gravity is taken into account during the interaction. This model describes both the contact dynamic of all bounces and the bead oscillations on the plane.

The different mechanisms of energy loss occurring during impact have been discussed. We have emphasized that at low impact velocity, these energy losses are essentially due to viscoelastic dissipation. A dissipative numerical model, based on a viscoelastic mechanism, leads to an evolution of the restitution coefficient identical to the experimental one. Besides, we have underlined that the strong decrease of the restitution coefficient as $v_{imp} \to 0$ did not come from a new dissipative mechanism, but from the fact that the system dissipates energy in a different way: When the gravity force is prominent compared to the elastic force, the system dissipates more energy than when the gravity force is negligible during the interaction.

This phenomenon does not allow to answer the question about the limit of the restitution coefficient, ϵ, in the limit of zero impact velocity. The measurement of the behavior of ϵ, when $v_{imp} \to 0$, is in preparation in low–gravity environment. We hope that this latter will allow to know if the collision between two spheres becomes perfectly elastic, *i.e.*, $\epsilon \to 1$, in the limit of zero velocity, or if a finite dissipation subsists in this limit, due to the singularity at the very beginning of the collision (high speed initial deformation even at low impact velocity [57]).

Finally, this work also shows that the collisional singularity is smoothed before leading to a new regime at the end of the bouncing process. Similarly, one might expect no measurable signature of the numerically observed inelastic collapse in any experiment.

We gratefully acknowledge financial support from the MENESR through the French laboratories network GEO and from the CNES through contrat 96/0318.

References

1. H.M. Jaeger, S.R. Nagel, R.P. Behringer, Rev. Mod. Phys. **68**, 1259 (1996).
2. H.M. Jaeger, S.R. Nagel, Science **255**, 1523 (1992).
3. C. Laroche, S. Douady, S. Fauve, J. Phys. France **50**, 699 (1989).
4. J.B. Knight *et al.*, Phys. Rev. E **54**, 5726 (1996), and references therein.
5. S. Fauve, S. Douady, C. Laroche, J. Phys. Colloq. France **50**, C3 187 (1989).
6. G.B. Lubkin, Phys. Today **48**, 17 (1995).
7. P.B. Umbanhowar, F. Melo, H.L. Swinney, Nature **382**, 793 (1996).
8. S. Luding *et al.*, Phys. Rev. E **49**, 1634 (1994).
9. S. Warr, J.M. Huntley, G.T.H. Jacques, Phys. Rev. E **5**, 5583 (1995).
10. A. Goldshtein, M. Shapiro, L. Moldavsky, M. Fichman, J. Fluid Mech. **287**, 349 (1995).
11. F.G. Bridges, A. Hatzes, D.N.C. Lin, Nature **309**, 333 (1984).
12. A.P. Hatzes, F.G. Bridges, D.N.C. Lin, Mon. Not. R. Astr. Soc. **231**, 1091 (1988).
13. K.D. Supulver, F.G. Bridges, D.N.C. Lin, Icarus **113**, 188 (1995).
14. C.K.K. Lun, S.B. Savage, Acta Mech. **63**, 15 (1986).
15. P.K. Haff, J. Fluid Mech. **134**, 401 (1983).
16. C.S. Campbell, Ann. Rev. Fluid Mech. **22**, 57 (1990).
17. J. Lee, Physica A **219**, 305 (1995).
18. S. McNamara, W.R. Young, Phys. Rev. E **53**, 5089 (1996).
19. I. Goldhirsch, G. Zanetti, Phys. Rev. Lett. **70**, 1619 (1993).
20. S. McNamara, W.R. Young, Phys. Fluids A **4**, 496 (1992).
21. B. Bernu, R. Mazighi, J. Phys. A **23**, 5745 (1990).
22. P. Constantin, E. Grossman, M. Mungan, Physica D **83**, 409 (1995).
23. S. McNamara, W.R. Young, Phys. Rev. E **50**, R28 (1994).
24. E. Falcon, C. Laroche, S. Fauve, C. Coste, submitted to Eur. Phys. J. B.
25. J.A. Zukas, T. Nicholas, *Impact Dynamics* (Wiley, New York, 1982).
26. K.L. Johnson, *Contact Mechanics* (Cambridge Univ. Press, Cambridge, 1985).

27. W. Goldsmith, *Impact* (Arnold, London, 1960).
28. C.V. Raman, Phys. Rev. **12**, 442 (1918).
29. S.C. Hunter, J. Mech. Phys. Solids **5**, 162 (1957).
30. J. Reed, J. Phys. D **18**, 2329 (1985).
31. J.P.A. Tillett, Proc. Phys. Soc. B **67**, 677 (1954).
32. M.G. Koller, H. Kolsky, Int. J. Solids Structures **23**, 1387 (1987).
33. R. Sondergaard, K. Chaney, C.E. Brennen, ASME J. Appl. Mech. **57**, 694 (1990).
34. C. Zener, Phys. Rev. **59**, 669 (1941).
35. D. Tabor, Proc. Roy. Soc. A **192**, 247 (1948).
36. Y.M. Tsai, H. Kolsky, J. Mech. Phys. Solids **15**, 263 (1967).
37. J.M. Lifshitz, H. Kolsky, J. Mech. Phys. Solids **12**, 35 (1964).
38. G. Kuwabara, K. Kono, Jap. J. Appl. Phys. **26**, 1230 (1987).
39. L.D. Landau, E.M. Lifshitz, *Theory of elasticity*, 3rd ed. (Pergamon Press, Oxford, 1986).
40. S.F. Foerster, M.Y. Louge, H. Chang, K. Allia, Phys. Fluids **6**, 1108 (1994).
41. A.D. Bernstein, Am. J. Phys. **45**, 41 (1977).
42. A.D. Bernstein, Am. J. Phys. **46**, 952 (1978).
43. P.A. Smith, C.D. Spencer, D.E. Jones, Am. J. Phys. **49**, 136 (1981).
44. *American Institute of Physics Handbook*, 3rd ed., edited by D.E. Gray (McGraw–Hill, New–York, 1972).
45. see Table 11.3 page 366 in Ref. [26].
46. O.R. Walton, in *Particulate two–phase flow*, edited by M.C. Roco (Butterworth–Heinemann, Boston, 1993) p. 884–911.
47. J. Lee, J. Phys. A **27**, L257 (1994).
48. Y.-H. Taguchi, Phys. Rev. Lett. **69**, 1367 (1992).
49. Y.-H. Taguchi, J. Phys. II France **2**, 2103 (1992).
50. J. Schäfer, S. Dippel, D.E. Wolf, J. Phys. I France **6**, 5 (1996).
51. S. Luding *et al.*, Phys. Rev. E **50**, 4113 (1994).
52. J.-M. Hertzsch, F. Spahn, N.V. Brilliantov, J. Phys. II France **5**, 1725 (1995).
53. N.V. Brilliantov, F. Spahn, J.-M. Hertzsch, T. Pöschel, Phys. Rev. E **53**, 5382 (1996).
54. E. Falcon, Ph.D. thesis, Université Claude Bernard Lyon I, 1997.
55. I.S. Gradshteyn, I.M. Ryzhik, in *Table of Integrals, Series, and Products*, 5 ed., edited by A. Jeffrey (Academic Press, London, 1965).
56. J.P. Dilley, Icarus **105**, 225 (1993).
57. J.C. Thompson, A.R. Robinson, ASME J. Appl. Mech. Series E **44**, 583 (1977).